

UCSF

UC San Francisco Previously Published Works

Title

Biochemical Basis for Distinct Roles of the Heterochromatin Proteins Swi6 and Chp2

Permalink

<https://escholarship.org/uc/item/97b8n7bt>

Journal

Journal of Molecular Biology, 429(23)

ISSN

0022-2836

Authors

Isaac, R Stefan

Sanulli, Serena

Tibble, Ryan

et al.

Publication Date

2017-11-01

DOI

10.1016/j.jmb.2017.09.012

Peer reviewed



Published in final edited form as:

J Mol Biol. 2017 November 24; 429(23): 3666–3677. doi:10.1016/j.jmb.2017.09.012.

Biochemical basis for distinct roles of the heterochromatin proteins Swi6 and Chp2

R. Stefan Isaac^{1,2}, Serena Sanulli^{3,4}, Ryan Tibble^{3,4}, Michael Hornsby⁴, Matthew Ravalin⁴, Charles S. Craik⁴, John D. Gross^{3,4}, and Geeta J. Narlikar¹

¹Department of Biochemistry and Biophysics, University of California, San Francisco, San Francisco, United States

²Tetrad Graduate Program, University of California, San Francisco, San Francisco, United States

³Program in Chemistry and Chemical Biology, University of California, San Francisco, San Francisco, United States

⁴Department of Pharmaceutical Chemistry, University of California, San Francisco, San Francisco, United States

Abstract

Heterochromatin protein 1 (HP1) family proteins are conserved chromatin binding proteins involved in gene silencing, chromosome packaging, and chromosome segregation. These proteins recognize histone H3 lysine 9 methylated tails via their chromodomain (CD) and recruit additional ligand proteins with diverse activities through their dimerization domain, the chromoshadow domain (CSD). Species that have HP1 proteins possess multiple paralogs that perform non-overlapping roles *in vivo*. How different HP1 proteins, which are highly conserved, perform different functions is not well understood. Here, we use the two *Schizosaccharomyces pombe* HP1 paralogs, Swi6 and Chp2, as model systems to compare and contrast their biophysical properties. We find that Swi6 and Chp2 have similar dimerization and oligomerization equilibria, and that Swi6 binds slightly (~3-fold) more strongly to nucleosomes than Chp2. Further, while Swi6 binding to the H3K9me3 mark is regulated by a previously described auto-inhibition mechanism, the binding of Chp2 to the H3K9me3 mark is not analogously regulated. In the context of CSD interactions, we show using a newly identified peptide sequence from the Clr3 histone deacetylase and a previously identified sequence from the protein Shugoshin that the Swi6 CSD binds both ligands more strongly than the Chp2. Overall, our findings uncover quantitative differences in how Swi6 and Chp2 interact with nucleosomal and non-nucleosomal ligands and qualitative differences

Publisher's Disclaimer: This is a PDF file of an unedited manuscript that has been accepted for publication. As a service to our customers we are providing this early version of the manuscript. The manuscript will undergo copyediting, typesetting, and review of the resulting proof before it is published in its final citable form. Please note that during the production process errors may be discovered which could affect the content, and all legal disclaimers that apply to the journal pertain.

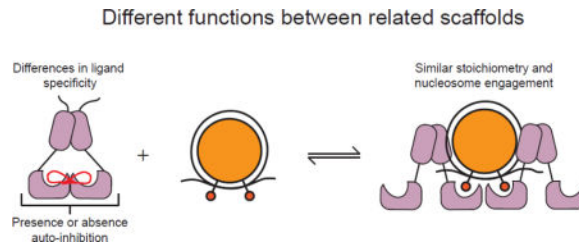
Author Contributions: R.S.I. and G.J.N. conceived of the core questions of this study. S.S. and R.T. performed the NMR experiments. R.T. and J.D.G. determined backbone assignments of the Swi6 CSD. R.S.I. performed the bulk of the biochemical experiments. R.S.I. and M.H. performed the phage display experiments. R.S.I. and M.R. carried out peptide synthesis and purification. R.S.I. and G.J.N. wrote the manuscript with significant contributions from S.S., R.T., and J.D.G.

Accession Numbers

Backbone assignments of the Swi6 CSD have been deposited in the Biological Magnetic Resonance Data Bank, accession number 27145. NMR chemical perturbations were mapped onto the Swi6 chromoshadow crystal structure with the PDB ID code 1E0B.

in how their assembly on nucleosomes is regulated. These findings provide a biochemical framework to explain the varied functions of Chp2 and Swi6 *in vivo*.

Graphical abstract



Keywords

Schizosaccharomyces pombe; heterochromatin; nuclear magnetic resonance (NMR); analytical ultracentrifugation

Introduction

Large regions of eukaryotic genomes are organized into heterochromatin, which is generally inaccessible to RNA polymerase and, therefore, is transcriptionally silenced. In addition to gene silencing, heterochromatin is also important for proper centromere function, repression of recombination, sister chromatid cohesion, and telomere stability^{1–4}. One specific type of heterochromatin is dependent on di- and tri-methylation of histone H3 at lysine 9 (H3K9me2/3), and this type of heterochromatin is conserved from fission yeast to humans⁵.

In the fission yeast *Schizosaccharomyces pombe*, heterochromatin is assembled on pericentromeric repeats, subtelomeric regions, the silent mating type locus, and rDNA¹. Establishment and maintenance of this silencing is dependent on several proteins including the H3K9 methyltransferase Clr4, histone deacetylases such as Clr3, and the heterochromatin protein 1 family proteins Swi6 and Chp2^{6–8}. HP1 proteins contain two globular domains: an N-terminal chromodomain (CD) that specifically recognizes H3K9me2/3 via an aromatic cage and a C-terminal chromoshadow domain (CSD) that dimerizes and recognizes various binding partners. These structured domains are connected by an unstructured, charged hinge region (H) that nonspecifically binds DNA and RNA^{8–11}.

Organisms that possess HP1 proteins generally have multiple paralogs that perform non-overlapping functions *in vivo*. For example, humans have three HP1 paralogs: HP1 α , HP1 β , and HP1 γ . HP1 α and HP1 β localize to heterochromatic loci and are involved in gene silencing. In contrast, HP1 γ localizes to euchromatic regions and has roles in transcriptional elongation and RNA processing^{12–15}. This supports the idea that these proteins have evolved to be general chromatin regulators involved in multiple nuclear processes. In *S. pombe*, both Swi6 and Chp2 are involved in the regulation of silent, H3K9me2/3-dependent heterochromatin, but they appear to have different roles; neither protein is able to rescue the loss of silencing phenotype in a deletion strain of the other⁸. In addition, establishing *de novo* heterochromatin by artificially recruiting the methyltransferase Clr4 requires Chp2 but

not Swi6¹⁶. Some of the differences in the biological roles of Swi6 and Chp2 could arise from differences in their intrinsic biophysical properties. Previous biochemical work identified an auto-inhibition based mechanism that regulates the binding of Swi6 to the H3K9me mark. This auto-inhibition arises because a loop with the sequence ARK in one chromodomain binds to the aromatic cage of the chromodomain in the other monomer. It is not known if binding of Chp2 to the H3K9me mark is similarly regulated. Swi6 and Chp2 are also known to have different binding partners, and it is possible that some of the biological differences can be explained by different binding preferences. Published IP-MS data showed Swi6 associating with numerous nuclear proteins, whereas Chp2 primarily pulled down components of the Snf2/HDAC-containing repressor complex (SHREC)^{7,8,17}. By *in vitro* pulldown assays with full-length proteins, it was shown that both Swi6 and Chp2 physically associate with the putative demethylase Epe1 and the histone deacetylase Clr3, albeit with different affinities⁸. Additionally, Swi6, but not Chp2, has been shown to bind the meiosis-specific protein Sgo1, and the interacting region was narrowed down by yeast two-hybrid¹⁸.

To directly test if Swi6 and Chp2 display differences in ligand specificity we compared the ability of their CSD domains to bind specific sequences from the Sgo1 and Clr3 proteins by NMR spectroscopy. Additionally, while much is known about the biochemical and biophysical properties of Swi6, little is known about the biophysical properties of the Chp2 paralog. We therefore also compared the nucleosome binding and oligomerization properties of Chp2 to those of Swi6. Together, these results indicate substantial differences in ligand specificity between Swi6 and Chp2 and suggest that Chp2 binding to H3K9me nucleosomes is not subject to Swi6-like auto-regulation. These intrinsic biophysical differences provide starting points to explain the different biological roles of Chp2 and Swi6.

Results

The chromoshadow domains of Swi6 and Chp2 show specificity differences for non-nucleosomal ligands

HP1 proteins have been proposed to act as platform molecules that recruit diverse activities to heterochromatic regions^{1,17,19–22}. The best-characterized HP1 domain that is known to recruit non-nucleosomal ligands is the CSD. Previously, the CSD domain of *D. melanogaster* HP1a was found to bind a “PXVXL” consensus motif, and this motif was found in a number of known HP1 interacting partners²³. To date, the binding motifs between different HP1 paralogs have not been compared. The center position valine was originally proposed to be strictly required, but a recent study has proposed relaxing this motif to $\Phi X(V/P)X\Phi$ based on binding of the human HP1 paralogs to a peptide from histone H3, where Φ denotes α -amino acids without side chain nitrogen or oxygen atoms²⁴. In *S. pombe*, one of the known binding partners of Swi6 is the Shugoshin 1 protein (Sgo1), and yeast two-hybrid experiments narrowed this interaction to the CSD of Swi6 and a peptide in Sgo1 resembling the $\Phi X(V/P)X\Phi$ motif, VCVCI. Mutations in either the C-terminal extension (CTE) of the CSD of Swi6 (F324, Figure 1A, Supplemental Figure 1A) or the VCVCI motif abrogated this interaction¹⁸. To investigate whether additional sequences

beyond those described by the $\Phi X(V/P)X\Phi$ motif could be accommodated within the CSD-CSD interface, we performed phage display with the CSDs of both Swi6 and Chp2.

We used a randomized nonapeptide library presented on the pVIII capsid protein of the filamentous phage M13 to compare recognized motifs between Swi6 and Chp2. We used Multiple EM for Motif Elicitation (MEME) analysis to discover sequence motifs in the identified peptides²⁵. Analysis of these motifs did not strongly indicate specific residues at any position. Rather, the results suggested a degenerate motif skewed toward hydrophobic and aliphatic residues (Supplemental Figure 2A and 2B). We then searched the *S. pombe* proteome for proteins containing this degenerate motif, specifically focusing on known physical and genetic interactors with Swi6 and Chp2. We tested binding of 24 peptides from selected proteins by fluorescence anisotropy. While the majority of the peptides did not show binding at the highest Swi6 and Chp2 concentrations that we tested (900 μM), we identified one binding partner for Swi6: a peptide from the type II histone deacetylase, Clr3. This peptide is contained in the C-terminal region of Clr3, which appears unstructured in a recent crystal structure of Clr3 (PDB ID 5IKK)²⁶. The sequence of this peptide contains “LLHLL”, which is distinct from the PXVXL motif and conforms to the $\Phi X(V/P)X\Phi$ more loosely than the Sgo1 peptide. We then compared affinities of Swi6 and Chp2 for the Sgo1 and Clr3 derived peptides.

To date, there is no evidence that Chp2 directly interacts with Sgo1. To assess the binding of Swi6 and Chp2 to this region of Sgo1, we measured binding to a peptide containing the “VCVCI” sequence in Sgo1 using fluorescence anisotropy (Figure 1B). Swi6 bound to this Sgo1 peptide with a K_d of $6.6 \mu\text{M} \pm 2.1$. The Swi6 CSD alone bound the peptide with the same K_d within error (9.8 ± 1.4), indicating that the major interaction of this peptide is with the CSD. Consistent with previous studies, saturable binding was not observed with a Swi6 CTE deletion even up to a concentration of $200 \mu\text{M}$ ¹⁸. Additionally, the V to E mutation previously tested by yeast two-hybrid greatly reduced Swi6 binding. In comparison, Chp2 bound 8.8-fold weaker to the Sgo1 peptide with a K_d of $58.5 \mu\text{M}$.

To examine the structural basis for this interaction, we applied NMR spectroscopy. NMR is a powerful tool for binding studies because of its sensitivity in monitoring changes in the chemical environment of amide bonds corresponding to the protein backbone and sidechains upon ligand binding. This allows us to examine even weak protein-protein interactions at high resolution and evaluate structural, thermodynamic, and kinetic aspects of the binding reaction. To this end, we first determined backbone assignments for the Swi6 CSD using standard triple resonance methods and the NMRFAM PINE Server²⁷.

Following the backbone assignment of the CSD, we performed ^1H - ^{15}N HSQC (Heteronuclear Single Quantum Correlation) NMR experiments with Swi6 and Chp2 CSDs in the presence of unlabeled Sgo1 peptide. Binding of the Sgo1 peptide showed numerous chemical shift perturbations (CSP) in the Swi6 CSD (Figure 1C, Figure 1E, Supplemental Figure 1A, Supplemental Figure 2C). Since the crystal structure of Swi6 CSD is available (PDB ID 1E0B)¹⁰, we were able to map the CSPs on the CSD structure and observe that they localize to the dimer interface, regions flanking this interface, and to residues in the CTE. The observed localization in chemical shift changes along a cleft formed by the CSD

dimer is consistent with where interacting peptides have been shown to bind in other HP1 proteins^{28–30}. Importantly, as previously observed by yeast two-hybrid, mutating the peptide motif to “VCECI” did not show any resonance changes by NMR (Supplemental Figure 2E). We next examined binding of the Sgo1 peptide to the Chp2 CSD. In contrast to the shifts observed with the Swi6 CSD, resonances were predominantly broadened with the addition of peptide to the Chp2 CSD (Supplemental Figure 3A). We observed some resonances that broaden below detection at low peptide concentration and reappear at a different chemical shift when a large excess of peptide was added. This precluded quantification of the K_d . The increased concentrations required for saturation compared to Swi6 suggest a weaker binding of the Sgo1 peptide to Chp2, which is consistent with our fluorescent anisotropy binding results (Figure 1B).

We next analyzed the Clr3 peptide derived from our phage display experiments. Both Swi6 and Chp2 were previously shown to physically interact with Clr3 by IP studies^{8,31}, but the region of Clr3 that interacts with Swi6 or Chp2 was not identified. To characterize the interaction of the Clr3 peptide with Swi6 and Chp2, we again turned to ¹H-¹⁵N HSQC NMR. Similar to binding of the Sgo1 peptide, binding of this Clr3 peptide to Swi6 caused chemical shift perturbations in residues mapping to the dimer interface, the regions flanking this interface, and the CTE (Figure 1D and 1E, Supplemental Figure 2C). Similar to the Sgo1 peptide, these residues overlay with the region known to interact with binding partners. These results directly demonstrate the specific region of Clr3 that physically interacts with Swi6. A K_d for this interaction was obtained by performing a series of titrations with increasing concentrations of Clr3 peptide. The observed chemical shift changes were plotted as a function of Clr3 concentration and fitted to a hyperbolic function to determine a K_d of $68 \pm 15 \mu\text{M}$, roughly 10.2-fold weaker than the affinity for the Sgo1 peptide (Figure 1D, Supplemental Figure 2D). This comparison suggests that the binding motifs recognized by HP1 proteins can be degenerate and that these sequence differences can lead to a broad range of binding affinities. Indeed, several CSD residues in this binding region are uniquely perturbed by either the Sgo1 or Clr3 peptide, suggesting different regions of the CSD are used for binding and this is dependent on ligand sequence (Figure 1E).

We next looked at the binding of the Clr3 peptide to the CSD of Chp2 and performed titration experiments with increasing concentration of peptide. Similar to the addition of the Sgo1 peptide, resonances broadened rather than shifted, indicating intermediate exchange. Although the K_d of this interaction cannot be reliably determined because of the major broadening, we were able to estimate the K_d by plotting the chemical shifts changes of two resonances as a function of Clr3 concentration (Supplemental Figure 3D). The preliminary fit to a hyperbolic function indicates a K_d in the high μM –low mM range. We also observed that binding saturation was achieved at higher concentrations of Clr3 peptide with the Chp2 CSD as compared to the Swi6 CSD. These observations indicate that the Chp2 binding to the Clr3 peptide is weaker than that of Swi6. Chp2 was previously suggested to have a higher affinity for full length Clr3 compared to Swi6 by IP⁸. It is possible that the weaker affinity of the peptide does not recapitulate binding of the full-length proteins, and that full-length Chp2 makes additional interactions with Clr3.

Together the results above suggest that differences in specificities of the Chp2 and Swi6 CSDs may contribute to their different biological roles.

Chp2 binding to the H3K9me3 mark is not regulated by auto-inhibition

In addition to differences in binding non-nucleosomal ligands, differences in interactions with chromatin could further inform on the varied roles of Chp2 and Swi6 *in vivo*. Previously, it was shown that the CD alone of both Swi6 and Chp2 binds the H3K9me3 tail peptide with affinities in the low μM range, although Chp2 bound the peptide tighter⁸. However, a detailed comparison of the interactions of full-length Swi6 and Chp2 with both tail peptide and nucleosomes has not been performed. Comparisons with full-length proteins are critical, especially considering mechanisms such as the observed Swi6 auto-inhibited state that is not present in the CD alone. The full-length Swi6 dimer has been shown to exist in both an open, binding competent state and a closed, auto-inhibited state³². This closed conformation is stabilized ~10-fold over the open state by an ARK loop in one chromodomain binding to the aromatic cage of the chromodomain in the other monomer. As the H3K9me3 peptide also binds in a similar location on the CD, binding of the ARK loop is mutually exclusive with binding to the H3 tail.

We wanted to determine if the Chp2 dimer also adopts an auto-inhibited, closed state. The chromodomains of Swi6 and Chp2 show a high degree of homology, with a sequence identity of 53% and a sequence similarity of 66.7%. Importantly, one of the sites of divergence in sequence lies within the ARK loop of Swi6; Chp2 instead has a KKD sequence (Supplemental Figure 1A). It is possible that the presence of this acidic residue prevents the domain swapping behavior of the Swi6 chromodomain. For Swi6, the presence of auto-inhibition in the Swi6 dimer was inferred, in part, by the finding that disrupting dimerization via the CSD-CSD interface resulted in increased binding for an H3K9me peptide³². This is because disrupting the CSD-CSD interface results predominantly in a monomer thereby disrupting the ARK loop-CD interaction. To test if Chp2 displays analogous auto-inhibition, we compared the affinity of WT and Chp2 I370E, a mutant that disrupts CSD dimerization, for H3K9me peptides. The CSD mutant resulted in Chp2 being predominantly a monomer up to 70 μM (Data not shown), yet this mutant bound the H3K9me peptide with comparable affinity as the WT dimeric protein (Supplemental Figure 6A), suggesting the absence of a Swi6 like auto-inhibitory mechanism in the WT Chp2 dimer.

In the context of Swi6, another way that auto-inhibition was previously disabled was via mutating the ARK loop³². This mutation increased the affinity of Swi6 for the H3K9me3 tail peptides but decreased the affinity for H3K9me3 nucleosomes³². This is because the ARK loop plays two roles: an auto-inhibitory role by directly competing with the H3K9me3 mark for binding the CD, and a stabilizing role via interactions with the nucleosome once it is displaced from the CD by the H3K9me3 mark³². Chp2 binds the H3K9me3 tail peptide with a K_d of 1.85 μM , ~5.5-fold tighter than Swi6 (Figure 2A). The Swi6 ARK loop mutant binds this peptide with a similar affinity to that of wild-type Chp2, consistent with the idea that Chp2 does not adopt an auto-inhibitory conformation³². Despite the differences in affinity for the H3K9me3 tail peptide, both Swi6 and Chp2 show substantial specificity for the

H3K9me3 mark as they both bind the unmethylated H3 tail peptide at least 10-fold more weakly than the H3K9me3 tail peptide (Figure 2A).

We next asked how the specificity for the H3K9 methyl mark and affinity are affected in the context of a nucleosome. To measure binding to nucleosomes we used a previously developed fluorescence anisotropy based assay (Supplemental Figure 4)^{32,33}. Similar to previous observations, we found that Swi6 binds H3Kc9me3 nucleosomes more strongly (>90-fold) than unmethylated nucleosomes (Figure 2A). We further found that Chp2 also binds H3Kc9me3 nucleosomes more strongly than unmethylated nucleosomes (Figure 2A, >17-fold). These results indicate that like Swi6, Chp2 also displays substantial specificity for the H3K9 methyl mark in the context of nucleosomes. In terms of absolute affinity, Chp2 binds H3Kc9me3 nucleosomes ~3-fold more weakly than Swi6 (K_d = 430 nM vs. 130 nM respectively). This weaker binding is comparable to the affinity of the Swi6 ARK loop mutant for H3Kc9me3 nucleosomes, further consistent with the conclusion that Chp2 lacks a Swi6-like auto-inhibition mechanism³².

In previous work, negative stain electron microscopy (EM) of CFP-tagged Swi6 showed 2D class averages consistent with both a closed, auto-inhibited conformation and an open, spreading-competent conformation³². To see if different conformation states of the Chp2 dimer could be observed, we visualized Chp2 by negative stain EM. 1,806 particles were manually picked and 2D class averages were calculated using RELION. The 2D class averages obtained are consistent a single predominant state that appears elongated (Supplemental figure 6). However, given the low resolution of negative stain EM, we cannot rule out the possibility that alternate conformations exist that we cannot detect. Our attempts to obtain corresponding EM data with untagged Swi6 were inconclusive due to the smaller size of Swi6 dimers (85.9 vs. 74.4 KDa for Chp2 vs. Swi6 dimers respectively).

Together, the tail peptide and nucleosome binding results presented here are consistent with the lack of a Swi6-like auto-inhibition mechanism in the context of Chp2.

The dimerization interfaces of Swi6 and Chp2 are important for nucleosome interactions

The affinity of both Swi6 and Chp2 for an H3Kc9me3 nucleosome is 0.13 μ M and 0.43 μ M, respectively (Figure 2A). Therefore, Swi6 binds H3Kc9me3 nucleosomes ~77-fold tighter than H3K9me3 tail peptide alone, and Chp2 binds H3Kc9me3 nucleosomes at least 4-fold tighter than for the H3K9me3 tail peptide alone. This suggests that regions of the protein other than the CD are also important for nucleosome binding. The hinge region of HP1 proteins has been shown to nonspecifically bind both DNA and RNA^{32,34}, suggesting that this region of Swi6 and Chp2 could bind the nucleosomal DNA. It is possible that other domains recognize the nucleosome as well. As mentioned in the first section, the CSD dimer can interact with other proteins through a cleft formed between the two monomers. To test whether an intact CSD dimer is important for nucleosome binding by Swi6 and Chp2, we measured nucleosome binding using two mutants, Swi6 L315D and Chp2 I370E, which substantially disrupt dimerization^{8,32,33}. Swi6 L315D and Chp2 I370E displayed a 8.5-fold and 3-fold weaker K_d for mononucleosomes, respectively (Figure 3B). These data suggest that an intact CSD-CSD interface is important for recognizing the nucleosome.

The dimerization and oligomerization equilibria for Chp2 and Swi6 are similar

A core property of heterochromatin is its ability to spread. It has been suggested that the spreading of heterochromatin arises in part due to the oligomerization of HP1 proteins^{1,17,19,22,31,33}. Previous work using analytical ultracentrifugation (AUC) has shown that Swi6 forms tight dimers ($K_{\text{dim}} < 6 \text{ nM}$ at 24°C) and weak higher order oligomers ($K_{\text{iso}} = 151 \text{ }\mu\text{M}$ at 24°C)^{32,33}. Similar measurements have not been carried out with Chp2 although previous qualitative comparisons using elution over a size-exclusion column have suggested that Chp2 is a weaker dimer than Swi6⁸.

To quantify the self-association of Chp2, we used sedimentation velocity analytical ultracentrifugation (SV-AUC). It is well known that the dimerization of HP1 proteins is mediated through the CSD, whereas it was previously shown that the tetramerization interface of Swi6 is through the N-terminal chromodomain³³. Similar to Swi6, Chp2 exhibits a tight association of two monomers with a dissociation constant K_{dim} of $< 3 \text{ nM}$ at 24°C. Further isodesmic association of Chp2 dimers has a dissociation constant K_{iso} of 183 μM at 24°C (Figure 2A). A comparison at 37 °C showed similar values for K_{iso} for Swi6 and Chp2 as well as a comparable K_{dim} value for Chp2 (Figure 2B, Supplemental figure 5). Thus overall, the dimerization and oligomerization equilibrium constants for Chp2 are comparable to those for Swi6.

Previously, it was shown by size exclusion chromatography that Chp2 elutes as two peaks with the slower peak corresponding to a monomer⁸. Given that we find that the equilibrium constants for dimerization are similar for Chp2 and Swi6, one possibility is that the on and off rates of Chp2 monomers differ from those of Swi6, resulting in Chp2 eluting as multiple peaks by SEC.

Chp2 binds nucleosomes with a stoichiometry of 4:1 similar to Swi6

In addition to the intrinsic ability of Swi6 to oligomerize, its stoichiometry on nucleosomes has suggested models for how Swi6 molecules can spread across chromatin. Specifically, previous work using sedimentation velocity analytical ultracentrifugation (SV-AUC) has shown that two Swi6 dimers bind a single nucleosome, leading to a “sticky end” model in which Swi6 is able to bridge adjacent nucleosomes³³. As Chp2 is lower in abundance in *S. pombe*⁸ and seems to have a less significant role in heterochromatin spreading^{8,16}, we wondered if only a single dimer of Chp2 binds a mononucleosome.

To determine the stoichiometry of the Chp2:Nucleosome complex, we used the same SV-AUC approach used previously for assessing the stoichiometry of the Swi6:Nucleosome complex³³. We performed SV-AUC with H3Kc9me3 nucleosomes alone, with wild-type Chp2, and with Chp2 I370E, a mutant that is unable to dimerize. Each experiment was analyzed using a $c(s)$ distribution with a fixed frictional coefficient (f/f_0) value as well as a bimodal f/f_0 distribution, where the frictional coefficient is a general measure of molecule shape.

These experiments showed that, analogous to Swi6, four Chp2 molecules bind a single nucleosome implying two dimers of Chp2. Consistent with this model, the Chp2 dimerization mutant bound with a stoichiometry of 2:1. As was hypothesized with Swi6,

these data suggest that Chp2 may also form “sticky ends” on mononucleosomes and bridge adjacent nucleosomes.

Discussion

Although much is known about the biochemical properties of individual HP1 proteins, less is known about the biochemical differences between paralogs and how these differences contribute to non-overlapping roles *in vivo*. In order to understand how paralogs vary in their intrinsic molecular behaviors, we characterized the biophysical properties of *S. pombe* HP1 protein Chp2 in comparison with Swi6. Both proteins are involved in H3K9me2/3-dependent heterochromatin, but genetically have been shown to have non-overlapping roles.

While the chromoshadow domains of Swi6 and Chp2 are homologous (40% sequence identity, 69% sequence similarity), they have been shown to bind different effector proteins. Indeed, one striking difference is that chimeras swapping the CSDs of Swi6 and Chp2 result in a loss of silencing phenotype⁸. Here we show that the Swi6 and Chp2 CSDs bind to peptides from Sgo1 and Clr3, although the affinities vary. Chp2, which is not known to bind Sgo1 *in vivo*, binds 6-fold more weakly to the Sgo1 peptide than Swi6. In contrast to Sgo1, Chp2 has been suggested to directly interact with Clr3, a histone deacetylase involved in heterochromatin formation. Yet compared to Swi6, Chp2 binds the Clr3 peptide at least 12-fold more weakly. It is possible that additional interactions with the full-length Clr3 protein stabilize binding between Chp2 and Clr3 *in vivo*. Importantly, this work identifies a specific region of Clr3 that directly interacts with Swi6 and Chp2. Together, these data are also consistent with recent studies that imply that the CSD binding motif is more degenerate than the PXVXL motif identified in early studies^{23,24}. These recent studies have suggested a relaxed motif of $\Phi X(V/P)X\Phi$ ²⁴. We speculate, given the peptides derived from our study, that the *S. pombe* HP1 proteins may tolerate additional deviations from the relaxed $\Phi X(V/P)X\Phi$ motif. It is also possible that the preferred binding motif differs across species. Further, amino acid differences between the CSDs of HP1 paralogs within a species may also contribute to different binding affinities for the same ligands. Such differences could explain in part why Swi6 and Chp2 interact with different proteins *in vivo* and in turn why they have different biological functions.

We also find that Chp2 binds ~3-fold more weakly to H3K9me3 nucleosomes than Swi6. It is unknown which portions of the Swi6 and Chp2 proteins specifically lead to this small binding difference. There are significant differences in sequence between both the NTE and the hinge between these proteins. It is known that the NTE of Swi6 contributes to histone H3 tail binding. The role of the Chp2 NTE, which is roughly half the size of the whole protein, is not known. Additionally, we show here and in previous work that dimerization of the CSDs of both Swi6 and Chp2 is important for nucleosome binding. This observation raises the possibility that the CSD-CSD dimer interface that interacts with non-nucleosomal ligands like Clr3 also plays a role in nucleosome binding. Indeed, it has recently been shown that CSDs of human HP1 α , HP1 β , and HP1 γ bind a peptide with the sequence PGTVAL from the globular portion of histone H3 with a K_d in the low μM range²⁴. However, we find that the Swi6 CSD binds this peptide with a substantially weaker affinity (Supplemental Figure 3E, $K_d > 1 \text{ mM}$). It is thus possible that the CSDs of Swi6 and Chp2 recognize a

different portion of the histone octamer. It is also unclear if the same region of the CSD that binds effector proteins also binds the nucleosome. This leads to interesting possible mechanisms with how Swi6 and Chp2 engage with the nucleosome and other proteins. For example, if the same region binds both the nucleosome and effectors, the CSD may not be able to simultaneously engage with both substrates. In this context, the ~3-fold weaker binding of Chp2 may make it slightly more prone than Swi6 to dissociate from nucleosomes if its CSD is bound by a non-nucleosomal ligand, raising the possibility that Swi6 is better suited than Chp2 to act as a platform for recruiting diverse activities while remaining bound to chromatin.

Our data also suggest that Chp2, unlike Swi6, does not adopt an auto-inhibitory conformation. Chp2's H3K9me3 peptide and nucleosome affinity parallel the properties of the uninhibited Swi6 ARK loop mutant. Yet, like Swi6, Chp2 can assemble as a tetramer on a mononucleosome and lead to a sticky ends architecture. This raises interesting questions about why Chp2 may not be subject to the same auto-regulation as Swi6. Swi6 is much more abundant *in vivo* than Chp2 (Roughly 20,000 molecules compared to 200 per cell)⁸. As it is involved in numerous nuclear processes, it is easy to imagine that multiple levels of regulation are required to prevent the ectopic assembly and spread of Swi6. The auto-inhibitory state of Swi6, which is mutually exclusive with higher-order oligomerization and nucleosome binding, provides a means for such regulation. Chp2 is much less abundant and seems to have a more specific role in heterochromatin establishment¹⁶. Therefore, we hypothesize it may not be necessary to regulate Chp2 binding and oligomerization to the same extent as Swi6, suggesting one explanation for the lack of a Swi6-like auto-inhibitory state. The lower nuclear concentration of Chp2 also suggests that, unlike with Swi6, the sticky ends architecture may not be used for spreading, but instead may be used for bridging across a proximal nucleosome, for interacting with Swi6 molecules, or for interacting with other binding partners.

HP1 proteins form a dynamic chromatin platform that can recruit effector proteins, and these proteins have likely evolved to suit their different roles within a given species. However, Swi6 and Chp2, as well as other HP1 proteins, interact with many different proteins, and most of these interfaces are unknown. Further studies will lead to a better understanding of which of these interactions are mediated via the CSD, which are mediated by other HP1 domains, how they regulate nucleosome binding and how they differ between paralogs and species.

Materials and Methods

Protein Cloning and Purification

Swi6 was purified from *Escherichia coli* as previously described^{32,33}. Chp2 was cloned into pET30a at the BamHI and NotI sites with a TEV cleavage site separating the 6xHis tag and the Chp2 coding sequence. Swi6 and Chp2 full-length proteins were purified from *E. coli* Rosetta (DE3) cells. Cells were grown to OD 0.6 at 37°C in LB medium with 50 µg/µL Kanamycin. Isopropyl-β-D-thiogalactopyranoside was added to a final concentration of 0.5 mM to induce protein expression, and cells were incubated at 18°C for 16 hours. Harvested cells were resuspended in lysis buffer (1X PBS buffer pH 7.8, 300 mM KCl, 10% glycerol,

7.5 mM imidazole, and protease inhibitors: phenylmethanesulfonyl fluoride, pepstatin A, aprotinin, and leupeptin). Following lysis in a C3 Emulsiflex (Avestin), cell debris was removed by centrifugation at 25,000g for 45 minutes. Clarified lysate was incubated with Cobalt-NTA affinity resin (Clontech) for 1 hour at 4°C. Resin was then washed and proteins were eluted with 20 mM Hepes pH 7.5, 100 mM KCl, 10% Glycerol, and 500 mM Imidazole. Proteins were cleaved overnight with 3 mg/mL TEV protease while dialyzing into 20 mM Hepes pH 7.5, 300 mM KCl, 1 mM DTT, and 10% glycerol. Protein was then purified by size-exclusion chromatography on a Superdex 200 26/60 column (GE Healthcare) with storage buffer (20 mM Hepes pH 7.5, 300 mM KCl, 1 mM DTT, 10% glycerol). For the CSDs of Swi6 and Chp2, a Superdex 75 16/60 column (GE Healthcare) was used for the size exclusion step. All N-terminal tags were cleaved using TEV protease except for NMR binding experiments involving the Chp2 CSD since the tag improved stability at NMR concentrations. Protein concentrations were measured by ultraviolet absorption at 280 nm and calculated using the extinction coefficient. Concentrations were measured by UV absorbance at 280 nm using the following calculated extinction coefficients: 40,910 M⁻¹ cm⁻¹ for full length Swi6, 8,480 M⁻¹ cm⁻¹ for Swi6 CSD, 55,350 M⁻¹ cm⁻¹ for full length Chp2, and 16,960 M⁻¹ cm⁻¹ for Chp2 CSD. To ensure that there was little to no DNA contamination, the 260/280 ratio was measured for each purified protein, which was 0.55 on average.

Nucleosome Reconstitution

Gradient salt dialysis was used to assemble mononucleosomes on DNA templates containing the 147 bp 601 sequence. Labeled nucleosomes were modified with a fluorescein tag on the 5' upstream end of the DNA. All nucleosomes were prepared using recombinant *Xenopus leavis* histones and assembled as previously described^{35,36}. Histone H3 containing methyl lysine analogue at position 9 (H3Kc9me3) were prepared as previously described³⁷.

Fluorescence Polarization—Fluorescence polarization binding assays to peptides and nucleosomes were performed in binding buffer (20 mM Hepes, 150 mM KCl, 1 mM DTT) supplemented with 0.02% NP-40 at 24°C. Substrates were used at a final concentration of 5 nM, and Swi6 and Chp2 concentrations were varied. The binding reaction was incubated for 30 minutes at 24°C. Fluorescence polarization was measured using an AnalystHT (Molecular Devices) with excitation and emission wavelengths of 480 and 530 nm, respectively.

The binding data were fit using the following equation:

$$FP_{obs} = \frac{[Protein] * FP_{max} + K_d * FP_{min}}{[Protein] + K_d}$$

In which FP_{obs} is the fluorescence polarization signal observed, FP_{min} is the fluorescence polarization signal for the probe alone, and FP_{max} is the fluorescence polarization signal at saturating protein concentration. The obtained K_d values were averaged over three or more independent sets of data.

Sedimentation Velocity Analytical Ultracentrifugation

Swi6 and Chp2 proteins were independently dialyzed into reaction buffer overnight at 4°C. All sedimentation velocity experiments were performed using an analytical ultracentrifuge (Beckman Coulter) equipped with an absorption optical scanner (Optima XLA). Data were acquired with ProteomeLab data acquisition software 5. Global analysis of sedimentation velocity isotherm data was performed using the SEDPHAT software. Partial-specific volume (v), solution density (ρ), and solution viscosity (η) were calculated in SEDNTERP.

Sample volumes of 100 μL or 400 μL at an overall final optical density (OD) between 0.1 and 1 were pipetted into double-sector centerpieces and places in an eight-hole rotor, which was then placed in a temperature equilibrated AUC chamber. An additional incubation of 1 to 2 hours was added with the rotor at rest and under vacuum for temperature equilibration. Runs were performed at a speed of 50,000 rpm. Scans were collected by following ultraviolet absorption at 230 nm, 250 nm, and 280 nm with a radial step size of 0.003 cm in continuous mode. Data were analyzed using a $c(s)$ continuous distribution of Lamm equation solutions with the SEDFIT software, following by integration and assembly into an isotherm of weighted-average s values. The isotherm was modeled in SEDPHAT with mass-action-based models for the weighted-average s value.

Nuclear Magnetic Resonance

For backbone assignment of the Swi6 CSD, protein was expressed in M9 minimal media containing ^{15}N -ammonium chloride and ^{13}C -glucose as the sole nitrogen and carbon source, respectively. Proteins were purified as previously described (above) with exchange into a final buffer containing 20 mM Hepes pH 7.8, 150 mM KCl, and 2 mM DTT. Backbone assignments were obtained from nitrogen HSQC and triple-resonance (HNCA, CBCA(CO)NH) experiments recorded at 303K on either a Bruker Avance DRX500 or Bruker Avance 800 MHz spectrometer equipped with cryogenic probes. For binding experiments, unlabeled peptides were added to either 100 μM ^{15}N -labeled Swi6 CSD or Chp2 His-tagged CSD and nitrogen HSQC spectra were recorded at 303K on a Bruker Avance DRX500 spectrometer. Chemical shift perturbations were calculated from the equation:

$$\sqrt{0.5 \left((\delta H_{bound} - \delta H_{free})^2 + (0.2 (\delta N_{bound} - \delta N_{free}))^2 \right)}$$

where the factor of 0.2 is used as a scaling factor for the nitrogen spectral width. Titration data were only fitted to obtain K_d values if the chemical shift perturbation between apo and final peptide concentration for a residue was greater than the mean plus one standard deviation.

Negative Stain Electron Microscopy and Image Processing—Chp2 protein was dialyzed overnight into sample buffer. 2.5 μL of Chp2 protein at 0.1 μM was adsorbed onto a glow discharged copper grid for 30 seconds followed by conventional negative stain with uranyl formate. Images were collected using a Tecnai T12 microscope (FEI company) with an LaB6 filament and operated at 120-kV accelerating voltage. All images were collected at

a magnification of 52kx with an UltraScan 4096 × 4096 pixel CCD camera (Gatan). All images were 2×2 pixel binned to the final pixel size of 4.42 Å. A total of 1,806 particles were selected and processed using Relion³⁸.

Phage Display

A randomized nonapeptide library (X9) fused to the pVIII protein of the phagemid vector pC89 was used for the phage display procedure³⁹. Screening of the library was performed as follows: 1 μM of biotinylated Swi6 or Chp2 CSD was bound to streptavidin magnetic beads in PBST (phosphate-buffered saline 0.2% BSA. After washing 3 times, the protein and phage were eluted with TEV protease. Logarithmic phase *E. coli* XL-1 Blue cells were infected by the eluate and the phage amplified using the helper phage M13KO7. The third and fourth panning rounds were used to infect *E. coli*, and 96 individual colonies from each round were picked and sequenced.

Peptides

Sgo1: EKAKTSNVCVCIPCKSAEQ

Mutant Sgo1: EKAKTSNVCECIPCKSAEQ

Clr3: RAVTQYLLHLLQKARPTSQ

H3 Tail Peptide: ARTKQTARKSTGGKA

Supplementary Material

Refer to Web version on PubMed Central for supplementary material.

Acknowledgments

We thank J. Tretyakova for the preparation of histone proteins and C. Stoddard for help with EM grid preparation, Swi6 EM studies, and RELION processing. We thank C. Stoddard, S. Johnson, R. Almeida for helpful discussion and feedback. This work was supported by National Institutes of Health (NIH) grants R01GM108455 to G.J.N., 5P41CA196276 to M.H., and R01GM104659 to C.S.C.

Abbreviations

SV-AUC	sedimentation velocity analytical ultracentrifugation
CD	chromodomain
CSD	chromoshadow domain
H	Hinge Domain
CTE	C-terminal extension
HP1	heterochromatin protein 1
H3K9me3	histone H3 lysine 9 trimethylation
IP-MS	Immunoprecipitation mass spectrometry
SHREC	Snf2/HDAC-containing repressor complex

EM	electron microscopy
NMR	nuclear magnetic resonance
HSQC	Heteronuclear Single Quantum Correlation spectroscopy

References

1. Grewal SIS, Jia S. Heterochromatin revisited. *Nat Rev Genet.* 2007; 8:35–46. [PubMed: 17173056]
2. Dillon N. Heterochromatin structure and function. *Biol Cell.* 2004; 96:631–637. [PubMed: 15519697]
3. Peng JC, Karpen GH. Epigenetic regulation of heterochromatic DNA stability. *Current Opinion in Genetics & Development.* 2008; 18:204–211. [PubMed: 18372168]
4. Gartenberg M. Heterochromatin and the cohesion of sister chromatids. *Chromosome Res.* 2009; 17:229–238. [PubMed: 19308703]
5. Hall IM. Establishment and Maintenance of a Heterochromatin Domain. *Science.* 2002; 297:2232–2237. [PubMed: 12215653]
6. Thon G, Verhein-Hansen J. Four chromo-domain proteins of *Schizosaccharomyces pombe* differentially repress transcription at various chromosomal locations. *Genetics.* 2000; 155:551–568. [PubMed: 10835380]
7. Motamedi MR, et al. HP1 Proteins Form Distinct Complexes and Mediate Heterochromatic Gene Silencing by Nonoverlapping Mechanisms. *Molecular Cell.* 2008; 32:778–790. [PubMed: 19111658]
8. Sadaie M, et al. Balance between Distinct HP1 Family Proteins Controls Heterochromatin Assembly in Fission Yeast. *Molecular and Cellular Biology.* 2008; 28:6973–6988. [PubMed: 18809570]
9. Jacobs SA, Khorasanizadeh S. Structure of HP1 chromodomain bound to a lysine 9-methylated histone H3 tail. *Science.* 2002; 295:2080–2083. [PubMed: 11859155]
10. Cowieson NP, Partridge JF, Allshire RC, McLaughlin PJ. Dimerisation of a chromo shadow domain and distinctions from the chromodomain as revealed by structural analysis. *Curr Biol.* 2000; 10:517–525. [PubMed: 10801440]
11. Zhao T, Heyduk T, Allis CD, Eissenberg JC. Heterochromatin protein 1 binds to nucleosomes and DNA in vitro. *J Biol Chem.* 2000; 275:28332–28338. [PubMed: 10882726]
12. Vakoc CR, Mandat SA, Olenchock BA, Blobel GA. Histone H3 Lysine 9 Methylation and HP1 γ Are Associated with Transcription Elongation through Mammalian Chromatin. *Molecular Cell.* 2005; 19:381–391. [PubMed: 16061184]
13. Hayakawa T, Haraguchi T, Masumoto H, Hiraoka Y. Cell cycle behavior of human HP1 subtypes: distinct molecular domains of HP1 are required for their centromeric localization during interphase and metaphase. *J Cell Sci.* 2003; 116:3327–3338. [PubMed: 12840071]
14. Smallwood A, et al. CBX3 regulates efficient RNA processing genome-wide. *Genome Res.* 2012; 22:1426–1436. [PubMed: 22684280]
15. Billur M, Bartunik HD, Singh PB. The essential function of HP1 beta: a case of the tail wagging the dog? *Trends in Biochemical Sciences.* 2010; 35:115–123. [PubMed: 19836960]
16. Kagansky A, et al. Synthetic Heterochromatin Bypasses RNAi and Centromeric Repeats to Establish Functional Centromeres. *Science.* 2009; 324:1716–1719. [PubMed: 19556509]
17. Fischer T, et al. Diverse roles of HP1 proteins in heterochromatin assembly and functions in fission yeast. *PNAS.* 2009; 106:8998–9003. [PubMed: 19443688]
18. Yamagishi Y, Sakuno T, Shimura M, Watanabe Y. Heterochromatin links to centromeric protection by recruiting shugoshin. *Nature.* 2008; 455:251–255. [PubMed: 18716626]
19. Haldar S, Saini A, Nanda JS, Saini S, Singh J. Role of Swi6/HP1 Self-association-mediated Recruitment of Clr4/Suv39 in Establishment and Maintenance of Heterochromatin in Fission Yeast. *Journal of Biological Chemistry.* 2011; 286:9308–9320. [PubMed: 21224386]
20. Aygun O, Grewal SIS. Assembly and Functions of Heterochromatin in the Fission Yeast Genome. *Cold Spring Harbor Symposia on Quantitative Biology.* 2011; 75:259–267.

21. Zhang K, Mosch K, Fischle W, Grewal SIS. Roles of the Ctr4 methyltransferase complex in nucleation, spreading and maintenance of heterochromatin. *Nat Struct Mol Biol.* 2008; 15:381–388. [PubMed: 18345014]
22. Sugiyama T, et al. SHREC, an Effector Complex for Heterochromatic Transcriptional Silencing. *Cell.* 2007; 128:491–504. [PubMed: 17289569]
23. Smothers JF, Henikoff S. The HP1 chromo shadow domain binds a consensus peptide pentamer. *Curr Biol.* 2000; 10:27–30. [PubMed: 10660299]
24. Liu Y, et al. Peptide recognition by heterochromatin protein 1 (HP1) chromoshadow domains revisited: Plasticity in the pseudosymmetric histone binding site of human HP1. *Journal of Biological Chemistry.* 2017; 292:5655–5664. [PubMed: 28223359]
25. Bailey TL, Elkan C. Fitting a mixture model by expectation maximization to discover motifs in bipolymers. 1994
26. Job G, et al. SHREC Silences Heterochromatin via Distinct Remodeling and Deacetylation Modules. *Molecular Cell.* 2016; 62:207–221. [PubMed: 27105116]
27. Bahrami A, Assadi AH, Markley JL, Eghbalian HR. Probabilistic Interaction Network of Evidence Algorithm and its Application to Complete Labeling of Peak Lists from Protein NMR Spectroscopy. *PLoS Comp Biol.* 2009; 5:e1000307–15.
28. Brasher SV, et al. The structure of mouse HP1 suggests a unique mode of single peptide recognition by the shadow chromo domain dimer. *EMBO J.* 2000; 19:1587–1597. [PubMed: 10747027]
29. Nietlispach D, Laue E, Thiru A, et al. Structural basis of HP1/PXVXL motif peptide interactions and HP1 localisation to heterochromatin. *EMBO J.* 2004; 23:489–499. *EMBO J.* DOI: 10.1038/sj.emboj.7600088 [PubMed: 14765118]
30. Kang J, et al. Mitotic centromeric targeting of HP1 and its binding to Sgo1 are dispensable for sister-chromatid cohesion in human cells. 2011; 22:1181–1190.
31. Yamada T, Fischle W, Sugiyama T, Allis CD, Grewal SIS. The Nucleation and Maintenance of Heterochromatin by a Histone Deacetylase in Fission Yeast. *Molecular Cell.* 2005; 20:173–185. [PubMed: 16246721]
32. Canzio D, et al. A conformational switch in HP1 releases auto-inhibition to drive heterochromatin assembly. *Nature.* 2013; 496:377–381. [PubMed: 23485968]
33. Canzio D, et al. Chromodomain-Mediated Oligomerization of HP1 Suggests a Nucleosome-Bridging Mechanism for Heterochromatin Assembly. *Molecular Cell.* 2011; 41:67–81. [PubMed: 21211724]
34. Keller C, et al. HP1Swi6 Mediates the Recognition and Destruction of Heterochromatic RNA Transcripts. *Molecular Cell.* 2012; :1–13. DOI: 10.1016/j.molcel.2012.05.009
35. Luger K, Rechsteiner TJ, Richmond TJ. Expression and purification of recombinant histones and nucleosome reconstitution. *Methods Mol Biol.* 1999; 119:1–16. [PubMed: 10804500]
36. Luger K, Rechsteiner TJ, Richmond TJ. Preparation of nucleosome core particle from recombinant histones. *Meth Enzymol.* 1999; 304:3–19. [PubMed: 10372352]
37. Simon MD, et al. The site-specific installation of methyl-lysine analogs into recombinant histones. *Cell.* 2007; 128:1003–1012. [PubMed: 17350582]
38. Scheres SHW. RELION: Implementation of a Bayesian approach to cryo-EM structure determination. *Journal of Structural Biology.* 2012; 180:519–530. [PubMed: 23000701]
39. Felici F, Castagnoli L, Musacchio A, Jappelli R, Cesareni G. Selection of antibody ligands from a large library of oligopeptides expressed on a multivalent exposition vector. *J Mol Biol.* 1991; 222:301–310. [PubMed: 1720463]

Highlights

- Swi6 and Chp2 play different roles in heterochromatin formation and maintenance
- Swi6 binds peptides from Sgo1 and Clr3 more strongly than Chp2
- Chp2 is not regulated by a Swi6-like auto-inhibition based mechanism
- Chp2 and Swi6 biophysical differences found here help explain *in vivo* differences

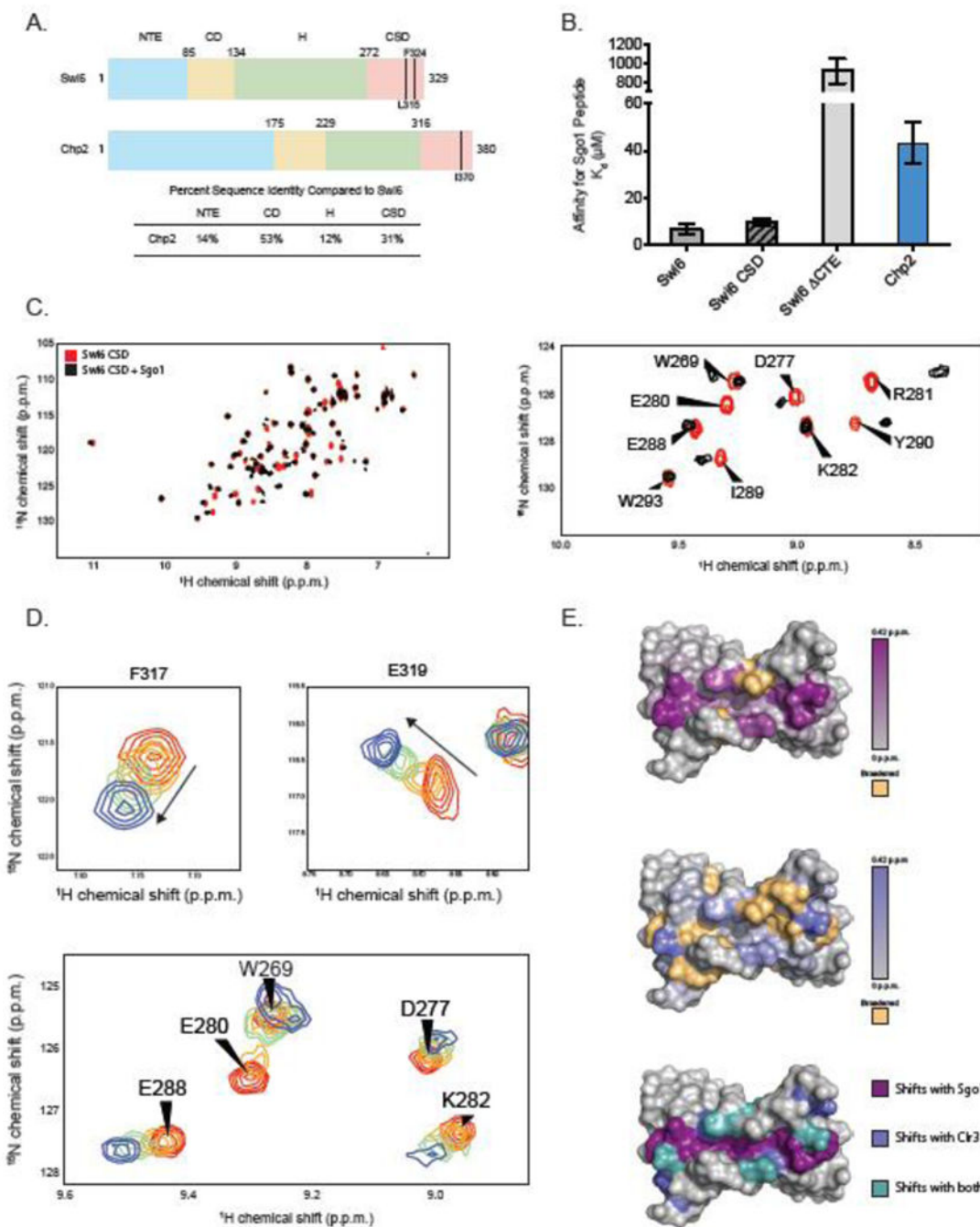




Figure 1.

(A) Domain schematic of Swi6 and Chp2 showing residue numbers and percent identity between the two proteins. Mutants used in these studies are indicated. Sequence identities were calculated using EMBOSS Needle. (B) Dissociation constants (K_d) for the Sgo1 peptide measured by fluorescence anisotropy. Experiments were carried out in triplicate at room temperature. (C) (Left) A superimposition of ^1H - ^{15}N HSQC spectra of Swi6 CSD with (black) and without (red) Sgo1 peptide. (Right) A zoom of a subset of chemical shift perturbations. (D) ^1H - ^{15}N HSQC spectra overlay of residues F317 and E319 while being

titrated by the Clr3 peptide. Concentrations of peptide shown are 0 μM (red), 20 μM (orange), 80 μM (green), 500 μM (blue). (E) The Swi6 CSD crystal structure colored by chemical shift perturbation upon the addition of 2X molar ratio Sgo1 peptide (Top) and 5X molar ratio Clr3 peptide (Middle). Orange indicates resonances that were broadened beyond detection upon peptide addition (PDB 1E0B). (Bottom) The Swi6 CSD crystal structure colored by shifts observed with Sgo1 peptide (purple), Clr3 peptide (blue), and with both peptides (teal).

A.

	H3 Tail Peptide Binding 		Nucleosome Binding 	
	H3K9me0 K_d (μ M)	H3K9me3 K_d (μ M)	H3K9me0 K_d (μ M)	H3Kc9me3 K_d (μ M)
WT Swi6	170 \pm 5	10 \pm 1.4	12 \pm 1.3	0.13 \pm 0.04
WT Chp2	>>20	1.85 \pm 0.15	>>7.44	0.43 \pm 0.17

B.

			T = 24°C		T = 37°C	
			Swi6	Chp2	Swi6	Chp2
Dimerization	$S + S$	$\xrightleftharpoons{K_{dim,obs}} S_2$	< 6 nM	< 3 nM	10 nM	14 nM
Isodesmic Self-Association	$S_2 + S_2$	$\xrightleftharpoons{K_{iso,obs}} S_4$	142 μ M	183 μ M	168 μ M	> 83 μ M

Figure 2.

(A) Characterization of H3 tail peptide binding and nucleosome binding with full-length Swi6 and Chp2 by fluorescence anisotropy. The 18 amino acid H3 tail peptide was N-terminally fluorescein labeled and had bona fide methylation at the K9 position. The nucleosomes were labeled on the 5' end of the 601 DNA. H3Kc9me3 nucleosomes were made by methyl lysine analog chemistry. All experiments were carried out in triplicate at room temperature. (B) Characterization of the self-association properties of WT Chp2. All experiments were performed at 24°C. Swi6 oligomerization values were previously reported in Canzio et al. 2013.

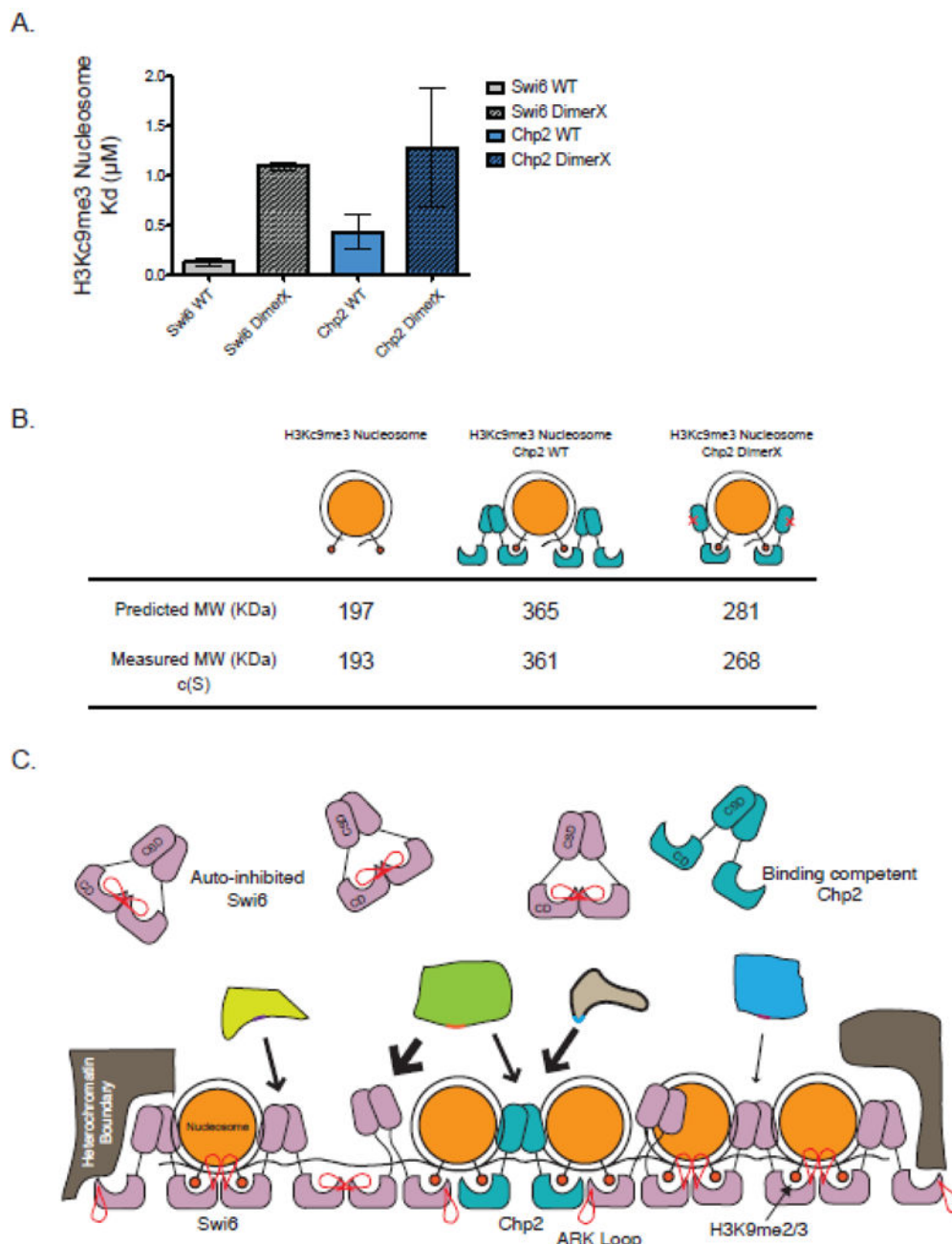


Figure 3. (A) Characterization of H3Kc9me3 core nucleosome binding with WT Swi6 and Chp2 as well as Swi6 and Chp2 dimerization mutants measured by fluorescence anisotropy. All experiments were carried out in triplicate at room temperature. (B) Average calculated masses and theoretical masses for H3Kc9me3 nucleosomes alone, with WT Chp2, and with Chp2 I370E as determined by SV-AUC using a continuous function $c(s)$ and an f/f_0 value of 1.6. (C) Model depicts differences in roles between the HP1 paralogs Swi6 (rose) and Chp2 (aqua). Paralogs recruit different effectors to chromatin due to differences in chromoshadow

peptide specificity and affinity. An excess of unbound Swi6 is regulated as an auto-inhibited conformation, whereas this does not exist in the lower abundant Chp2.

Author Manuscript

Author Manuscript

Author Manuscript

Author Manuscript